catalysts

Article

Enhanced Low Temperature NO Reduction Performance via MnO_x-Fe_2O_3/Vermiculite Monolithic Honeycomb Catalysts

Ke Zhang [1], Feng Yu [1,*], Mingyuan Zhu [1], Jianming Dan [1,2,3], Xugen Wang [1], Jinli Zhang [1] and Bin Dai [1,*]

1. Key Laboratory for Green Processing of Chemical Engineering of Xinjiang Bingtuan, School of Chemistry and Chemical Engineering, Shihezi University, Shihezi 832003, China; kezhang1014@163.com (K.Z.); zhuminyuan@shzu.edu.cn (M.Z.); djm_tea@shzu.edu.cn (J.D.); wxgen@shzu.edu.cn (X.W.); zhangjinli@tju.edu.cn (J.Z.)
2. Key Laboratory of Materials-Oriented Chemical Engineering of Xinjiang Uygur Autonomous Region, Shihezi 832003, China
3. Engineering Research Center of Materials-Oriented Chemical Engineering of Xinjiang Production and Construction Corps, Shihezi 832003, China

* Correspondence: yufeng05@mail.ipc.ac.cn (F.Y.); db_tea@shzu.edu.cn (B.D.); Tel.: +86-993-205-7272 (F.Y. & B.D.); Fax: +86-993-205-7270 (F.Y. & B.D.)

Received: 31 January 2018; Accepted: 27 February 2018; Published: 28 February 2018

Abstract: Selective catalytic reduction of NO_x by ammonia (NH_3-SCR) was the most efficient and economic technology for De-NO_x applications. Therefore, a series of MnO_x/vermiculite (VMT) and MnO_x-Fe_2O_3/VMT catalysts were prepared by an impregnation method for the selective catalytic reduction (SCR) of nitrogen oxides (NO_x). The MnO_x-Fe_2O_3/VMT catalysts provided an excellent NO conversion of 96.5% at 200 °C with a gas hourly space velocity (GHSV) of 30,000 h^{-1} and an NO concentration of 500 ppm. X-ray photoelectron spectroscopy results indicated that the Mn and Fe oxides of the MnO_x-Fe_2O_3/VMT catalyst were mainly composed of MnO_2 and Fe_2O_3. However, the MnO_2 and Fe_2O_3 components were well dispersed because no discernible MnO_2 and Fe_2O_3 phases were observed in X-ray powder diffraction spectra. Corresponding MnO_x-Fe_2O_3/VMT monolithic honeycomb catalysts (MHCs) were prepared by an extrusion method, and the MHCs achieved excellent SCR activity at low temperature, with an NO conversion greater than 98.6% at 150 °C and a GHSV of 4000 h^{-1}. In particular, the MnO_x-Fe_2O_3/VMT MHCs provided a good SCR activity at room temperature (20 °C), with an NO conversion of 62.2% (GHSV = 1000 h^{-1}). In addition, the NO reduction performance of the MnO_x-Fe_2O_3/VMT MHCs also demonstrated an excellent SO_2 resistance.

Keywords: MnO_x-Fe_2O_3/vermiculite; monolithic honeycomb catalyst; room-temperature catalysis; selective catalytic reduction; NO removal efficiency

1. Introduction

Nitrogen oxides (NO_x) in stationary stack source emissions are strong contributing factors of acid rain, photochemical smog, and ozone depletion and are, therefore, detrimental to the natural environment and human health [1–3]. Therefore, the selective catalytic reduction (SCR) of NO_x by ammonia (NH_3-SCR) was developed to reduce the release of NO_x (i.e., De-NO_x), and this has thus far been the most economical and effective technology for De-NO_x applications [4]. It is well known that the key component affecting the SCR and economic performance of NH_3-SCR technology is the catalyst employed in the process, which should be low in cost, and provide high SCR activity at low temperatures. As a result, manganese-based catalysts have been widely studied over the past few decades owing to their low cost and promisingly high SCR activity at low temperature [5]. However, the SCR activity of pure MnO_x catalysts is profoundly deteriorated by SO_2 and H_2O, and emissions with high concentrations of SO_2 and H_2O can lead to poisoning and the eventual deactivation of pure MnO_x catalysts. These drawbacks can be overcome, and the SCR activity of pure MnO_x catalysts can even be improved by incorporating transition metal or rare earth elements as catalyst promoters [6,7]. For example, Chen et al. reported that Fe-MnO_x mixed-oxide catalysts provided a 100% NO_x conversion in the temperature range from 140 °C to 220 °C [8].

Since SCR activity occurs on the surfaces of catalysts, the SCR activity of catalysts can be greatly enhanced, particularly under low-temperature conditions, by maximizing their surface area via distribution over high surface area supports. Numerous types of supports have been employed for Mn-based catalysts, such as molecular sieves, carbon materials, and metal oxides. Molecular sieves modified with Mn-based catalyst materials have shown excellent SCR activity because of their regular pore structures, high strength, and high specific surface areas [9]. Numerous Mn-based molecular sieve supported catalysts, such as Mn supported on ZSM-5 zeolite (denoted as Mn/ZSM-5) [10] and MnO_x/silicoaluminophosphate zeolite (SAPO-34) [11], have been shown to be highly active for NO_x reduction at low temperatures. Carbon materials have also been widely used as catalyst supports because of their well-developed porosity, high specific surface area, chemical stability, strong adsorption ability, and excellent thermal conductivity [12]. For example, Lu et al. synthesized MnO_2 supported on carbon nanotubes (CNTs), and the catalyst attained an NO conversion of 89.5% at 180 °C [13]. Finally, metal oxide supports provide high catalyst surface areas, high thermal stability, and surface acid-base properties [14,15]. Manganese-based catalysts supported on metal oxides, such as MnO_x/TiO_2 [16–18], MnO_x/Al_2O_3 [19], MnO_x/CeO_2 [20–22], and MnO_x/Ce-ZrO_2 [23], have generated considerable attention, and represent promising catalysts for the SCR of NO_x at low temperatures.

In recent years, many researchers have focused on catalysts employing supports composed of natural ore materials, such as montmorillonite, saponite, attapulgite, chabazite, and vermiculite (VMT), due to their great abundance, which makes them easily obtainable and inexpensive materials. A number of catalysts have incorporated these natural ore materials, such as Zr-Mn/attapulgite (ATP) [24], Ce-MnO_x/ATP [25], porous clay hetero-structures (PCH) modified with NH_3-Cu [26], Cu-chabazite (CHA) [27–29] and crystalline MnO_2 (c-MnO_2)/TiO_2-palygorskite (PAL) [30]. Among the available natural ore materials, the unique layered structure of VMT makes it an excellent candidate as a support for the SCR of NO. In addition, VMT includes metal oxides that can actively assist in catalytic reactions, and its great abundance in Xinjiang, China makes this material of particular interest to Chinese researchers. Chmielarz et al. investigated PCHs based on montmorillonite, saponite, and VMT modified with Fe or Cu as catalysts [31]. Among these catalysts, PCHs involving VMT achieved the best SCR activity at 400 °C. Samojeden et al. developed VMT supports prepared by modifications with nitric acid, and the resulting catalysts formed by impregnation with Cu provided an NO conversion of 94.3% at 350 °C [32]. Moreover, VMT has been widely investigated for use in heterogeneous catalysts, such as in the photocatalyst TiO_2/VMT [33], NiO/VMT for carbon monoxide methanation [34,35], and a novel $HgCl_2$/EML-VMT-C catalyst employing expanded multilayered (EML) VMT mixed with carbon on the surface (EML-VMT-C) for the hydrochlorination of acetylene [36]. However, the application of catalysts employing VMT supports for the SCR of NO_x at low temperatures remains challenging.

In light of the substantial cost benefits associated with the use of natural ore materials as catalyst supports, the present study employs VMT as supports in the fabrication of MnO_x-Fe_2O_3/VMT catalysts by the impregnation method for the SCR of NO by NH_3. The as-prepared MnO_x-Fe_2O_3/VMT catalysts provide an excellent NO conversion of 96.5% at 200 °C with a gas hourly space velocity (GHSV) of 30,000 h^{-1}. To improve the low temperature performance, corresponding MnO_x-Fe_2O_3/VMT monolithic honeycomb catalysts (MHCs) were prepared by an extrusion method, and the MHCs achieve an NO conversion greater than 98.6% at 150 °C and GHSV = 4000 h^{-1}. In particular, the MnO_x-Fe_2O_3/VMT MHCs provided good SCR activity at room temperature (20 °C), with an NO conversion of 62.2% (GHSV = 1000 h^{-1}). Finally, because flue gases still contain small amounts of

SO_2 after desulfurization and water removal, we also investigated the influence of SO_2 on the catalytic performance of MnO_x-Fe_2O_3/VMT MHCs.

2. Results and Discussion

The results of catalytic activity testing for the as-prepared MnO_x/VMT and MnO_x-Fe_2O_3/VMT catalysts are shown in Figure 1. As shown in Figure 1a, the NO conversion of the MnO_x/VMT and MnO_x-Fe_2O_3/VMT catalysts increased obviously with increasing temperature in the low temperature region until attaining a maximum value, after which the NO conversion decreased. The highest NO conversion attained for the MnO_x-Fe_2O_3/VMT catalyst was 96.5% at 200 °C, while the highest NO conversion attained for the MnO_x/VMT catalyst was 93.1% at 250 °C. Compared with the MnO_x/VMT catalyst, the catalytic activity of the MnO_x-Fe_2O_3/VMT catalyst was between 6% and 16% greater than that of the MnO_x/VMT catalyst in the low temperature range of 20–200 °C, indicating that the addition of Fe obviously increased the low temperature activity of the catalyst. For both catalysts, the declining NO conversion at relatively high temperatures originated from the oxidation of the ammonia.

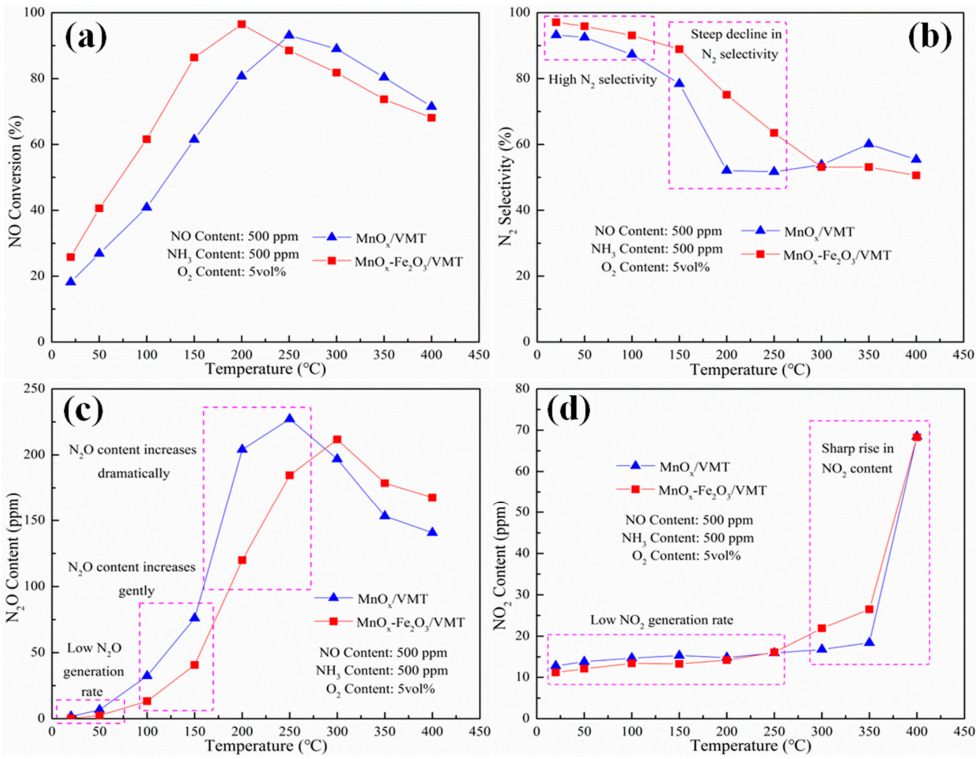

Figure 1. Catalytic activity of MnO_x/VMT and MnO_x-Fe_2O_3/VMT catalyst samples: (**a**) NO conversion; (**b**) N_2 selectivity; (**c**) N_2O content; and (**d**) NO_2 content (N_2 as balance gas, GHSV = 30,000 h^{-1}).

In addition, Figure 1b shows that the N_2 selectivity of the MnO_x/VMT and MnO_x-Fe_2O_3/VMT catalysts gradually declined with increasing temperature in the low temperature region (20–100 °C), and sharply declined in the middle temperature region (150–200 °C). The MnO_x-Fe_2O_3/VMT catalyst exhibited excellent N_2 selectivities of 97.1% and 95.9% at 20 °C and 50 °C, respectively, and its N_2 selectivity was greater than that of the MnO_x/VMT catalyst at temperatures less than 250 °C. However, we note that the sharp drop in the N_2 selectivity of the MnO_x-Fe_2O_3/VMT catalyst at 150 °C resulted in an N_2 selectivity that was less than that of the MnO_x/VMT catalyst at temperatures greater than 250 °C. The N_2 selectivity results are readily correlated with the measured N_2O and NO_2 contents shown in Figure 1c,d, respectively. Here, we note that the gradual decline in the N_2 selectivity of both catalysts at low temperature corresponds with a gradually increasing generation of N_2O and NO_2 over a similar temperature range. In addition, the sharply declining N_2 selectivity of both catalysts in the middle temperature region is mainly because the N_2O content is increasing rapidly for temperatures greater than 150 °C. We also note that the region over which the N_2 selectivity of the MnO_x/VMT catalyst was greater than that of the MnO_x-Fe_2O_3/VMT catalyst (i.e., at temperatures greater than 250 °C) corresponds with the fact that both the N_2O and the NO_2 contents were less for the MnO_x/VMT catalyst than for the MnO_x-Fe_2O_3/VMT catalyst at temperatures greater than 250 °C. Nevertheless, we note that the MnO_x-Fe_2O_3/VMT catalyst demonstrated both a better NO conversion and a better N_2 selectivity that those of the MnO_x/VMT catalyst in the temperature range of 20–200 °C.

Figure 2a presents X-ray diffractometer (XRD) patterns of the VMT support and as-prepared MnO_x/VMT and MnO_x-Fe_2O_3/VMT powdered catalyst samples. We note that VMT presents several strong peaks that exhibit greatly decreased intensities after impregnation. In addition, several diffraction peaks indicative of Mn_3O_4 (PDF#18-0803) are observed for the MnO_x/VMT catalyst at 18.1°, 29.2°, 32.4°, 36.2°, 51.0°, and 58.5°, while no others crystal phases of MnO_x are evident. These results suggest that the existence of diffraction peaks could be due to large crystals of MnO_x, resulting in weak XRD peaks indicative of MnO_x and VMT [37]. The MnO_x-Fe_2O_3/VMT catalyst sample presents even weaker XRD peaks indicative of MnO_x and VMT, and no additional crystal phases are observed. Here, the coexistence of manganese and iron oxides enhances dispersion, and consequently reduces the crystallinity, indicating the presence of strong interactions between these two metal oxides [38].

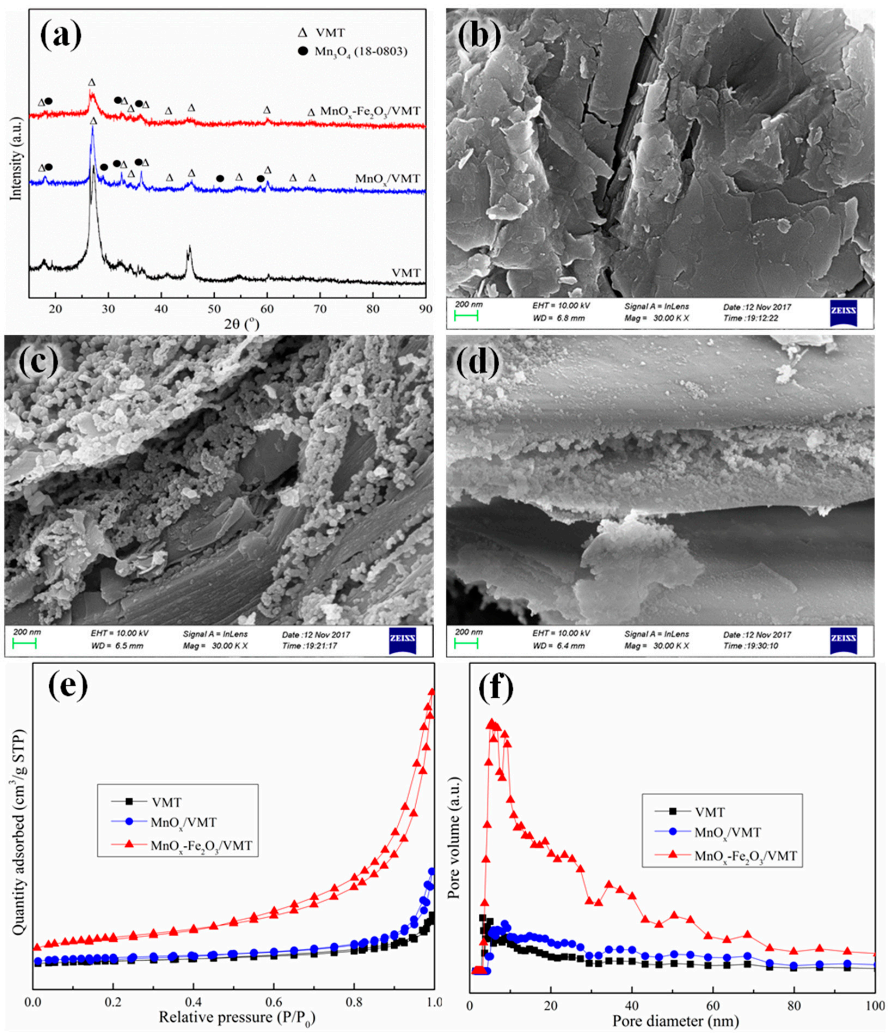

Figure 2. XRD patterns (**a**); N_2 isotherms (**b**) and pore diameter distribution curves (**c**); scanning electron microscopy (SEM) images (**d**–**f**) of the VMT support and MnO_x/VMT and MnO_x-Fe_2O_3/VMT catalyst samples.

Figure 2b–d present SEM micrographs indicative of the morphologies of the VMT support and as-prepared MnO_x/VMT and MnO_x-Fe_2O_3/VMT catalysts, respectively. We note the distinct layered structure of the VMT support, and that the layer surfaces are very smooth, without obvious pores or wrinkles. After impregnation, the MnO_x/VMT catalyst exhibits a distribution of irregular loose particles, and the layer surfaces of the VMT support appear to be very rough (Figure 2c), indicating the formation of many new channels on the VMT surfaces. However, the sizes of the irregular loose particles of the MnO_x-Fe_2O_3/VMT catalyst are substantially decreased. These results explain the reason for the increased surface area and decreased pore diameter of the MnO_x-Fe_2O_3/VMT catalyst relative to those of the MnO_x/VMT catalyst.

The N_2 adsorption-desorption isotherm plots and the corresponding BJH pore size distribution curves of the VMT support and as-prepared MnO_x/VMT and MnO_x-Fe_2O_3/VMT catalyst samples are presented in Figure 2e,f, respectively. From Figure 2e, we note the presence of well-defined type II hysteresis loops with sloping adsorption branches for all samples, which is particularly pronounced for the MnO_x-Fe_2O_3/VMT catalyst. From Figure 2f, we note that both catalyst samples exhibit three narrow peaks in the pore diameter range of 2–10 nm. The textural data for all samples are listed in Table 1. From the table, we find that the impregnation of 20 wt% Mn more than doubled the BET surface area of the MnO_x/VMT catalyst sample relative to that of the VMT support, but, surprisingly, the pore diameter decreased by about 30%. Moreover, the impregnation of 20 wt% Mn and 5 wt% Fe further increased the BET surface area of the MnO_x-Fe_2O_3/VMT catalyst sample by a factor greater than 3 relative to the MnO_x/VMT catalyst sample, while the pore diameter further decreased by about 12%. These results indicate that the doping of second metal can change the surface structure of the MnO_x-Fe_2O_3/VMT catalyst [39], and the calcination subsequent to impregnation may have formed additional channels in the surfaces of the VMT support. A high BET surface area is beneficial toward increasing the number of active sites of a catalyst and, thus, provides an increased NO conversion.

Table 1. Physical properties of VMT support and catalyst samples.

Samples	BET Surface Area (m^2/g)	Pore Volume (cm^3/g)	Pore Diameter (nm)
VMT support	2.9	0.02	26.2
MnO_x/VMT	6.7	0.03	18.4
MnO_x-Fe_2O_3/VMT	21.9	0.09	16.2
MnO_x-Fe_2O_3/VMT MHCs	15.4	0.07	17.9

The XPS spectra of the as-prepared MnO_x/VMT and MnO_x-Fe_2O_3/VMT catalysts are shown in Figure 3, and their principle surface compositions obtained from the fitted spectra in Figure 3b–d are listed in Table 2. Sharp photoelectron peaks are observed in Figure 3a for Fe, Mn, O, and C elements with binding energies of 712.1 eV (Fe $2p_{3/2}$), 642.1 eV (Mn $2p_{3/2}$), 532.1 eV (O 1s), and 284.1 eV (C 1s), respectively. We note that the XPS spectrum obtained for the MnO_x/VMT catalyst also exhibits a small peak indicative of Fe because the VMT support material naturally contains a small concentration of Fe. The Fe 2p, Mn 2p, and O 1s spectra of the catalyst samples are individually discussed in detail below.

Table 2. Surface compositions of representative catalyst samples obtained by XPS analysis.

Samples	Mn^{4+}/Mn_{total} (%)	O_{ads}/O_{total} (%)	Fe^{3+}/Fe_{total} (%)
MnO_x/VMT	26.3	38.5	51.5
MnO_x-Fe_2O_3/VMT	35.9	46.0	59.1

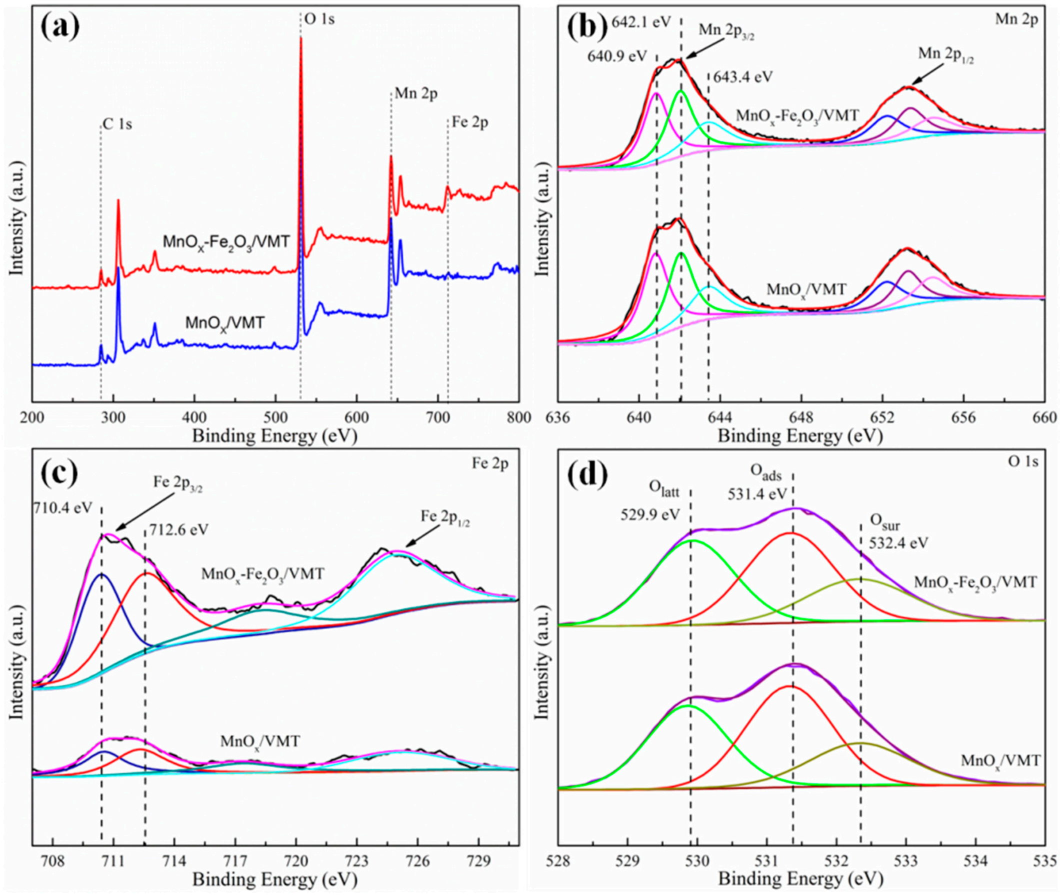

Figure 3. XPS survey spectra (**a**); Mn 2p spectra (**b**); Fe 2p spectra (**c**); O 1s spectra (**d**) of MnO_x/VMT and MnO_x-Fe_2O_3/VMT catalyst samples.

As shown in Figure 3b, the Mn 2p spectra include two main peaks at binding energies of 653.8 ± 0.4 eV and 641.9 ± 0.4 eV, which are assigned to Mn $2p_{3/2}$ and Mn $2p_{1/2}$ electron states, respectively. To identify the specific Mn species of each sample, the Mn $2p_{3/2}$ peak was deconvoluted into three peaks, corresponding to Mn^{2+} (641.0 ± 0.4 eV), Mn^{3+} (642.1 ± 0.4 eV), and Mn^{4+} (643.5 ± 0.4 eV), respectively [40]. The percentage of Mn atoms in the Mn^{4+} state listed in Table 2 was then determined as the area under the curve representative of Mn^{4+} relative to the total area under the Mn $2p_{3/2}$ curve. These values are indicative of the molar concentration of MnO_2 relative to all MnO_x on the surfaces of the MnO_x-Fe_2O_3/VMT and MnO_x/VMT catalysts. We note that the Mn^{4+} percentage increased by about 37% from the MnO_x/VMT catalyst to the MnO_x-Fe_2O_3/VMT catalyst. This indicates that the addition of Fe facilitates the conversion of MnO_x to MnO_2 on the catalyst surface. It has been reported [41–43] that the NO conversion capability of pure manganese oxides can be ranked as MnO_2 > Mn_5O_8 > Mn_2O_3 > Mn_3O_4. In addition, it has been reported that a greater concentration of MnO_2 on the catalyst surface promotes the SCR reaction [44]. Therefore, it can be expected that the MnO_x-Fe_2O_3/VMT catalyst will provide an improved NO conversion relative to that of the MnO_x/VMT catalyst.

The Fe 2p spectra presented in Figure 3c exhibit electron binding energy peak values for Fe $2p_{3/2}$ and Fe $2p_{1/2}$ states, and a satellite peak of 710.7, 725.0, and 718.6 eV, respectively. The satellite peak energy corresponds well with that reported for Fe_2O_3 [45]. The Fe $2p_{3/2}$ peak was deconvolved into two components with peaks at 710.4 eV and 712.6 eV indicative of Fe^{2+} and Fe^{3+} phases [46], respectively. The results indicate that the percentage of Fe atoms in the Fe^{3+} state listed in Table 2 are about 13% less in the VMT support of the MnO_x/VMT catalyst than that of the MnO_x-Fe_2O_3/VMT catalyst.

According to a past study [47], Fe^{3+} sites may facilitate the reduction of NO_x at low temperature. Thus, the MnO_x-Fe_2O_3/VMT catalyst can be expected to provide a slightly better low-temperature activity than that of the MnO_x/VMT catalyst.

As shown in Figure 3d the O 1s peaks of the MnO_x/VMT and MnO_x-Fe_2O_3/VMT catalysts at 528–535 eV were deconvolved into three peaks, denoted as O_{latt} (529.9 eV), O_{ads} (531.4 eV), and O_{sur} (532.4 eV), which are attributed to O atoms bonded with metal cations, in adsorbed water, and in surface hydroxyl groups, respectively [48]. It has been widely reported that oxygen in the gas phase can be activated by oxygen vacancies on the surface of SCR catalysts. Therefore, the relative abundance of O_{ads} is of particular interest because an increased percentage of O_{ads} can promote the oxidation of NO to NO_2, and enhance the SCR performance at low temperature through a rapid NH_3-SCR route [49,50]. As shown in Table 2, the ratio of O_{ads}/O_{total} on the surface of the MnO_x-Fe_2O_3/VMT catalyst is about 19% greater than that for the MnO_x/VMT catalyst. As a result, we can expect this factor to further enhance the low-temperature activity of the MnO_x-Fe_2O_3/VMT catalyst relative to that of the MnO_x/VMT catalyst.

The results of H_2-TPR testing are presented in Figure 4 for the VMT support and the as-prepared MnO_x/VMT and MnO_x-Fe_2O_3/VMT catalysts. We note that several peaks are observable for all samples within the temperature range of 200–800 °C. The H_2-TPR curve for the VMT support includes only two peaks, with a reduction peak attributed to $Fe_2O_3 \rightarrow Fe_3O_4$ at 274 °C, and a second peak located at 688 °C that may be attributed to $Fe_3O_4 \rightarrow FeO$ [51]. Compared with the VMT support curve, two new reduction peaks are observed in the H_2-TPR curve for the MnO_x/VMT catalyst due to the addition of Mn. From previous studies [52], the reduction peaks of MnO_x can be assigned to the reduction processes of MnO_2 via Mn_2O_3 to MnO. Here, the first peak observed at 269 °C can be attributed to the $MnO_2 \rightarrow Mn_2O_3$ reduction transition, while the peak at 469 °C can be attributed to $Mn_2O_3 \rightarrow MnO$ [53]. Therefore, because the MnO_x/VMT catalyst includes Fe_2O_3 in the support, the peak centered at 269 °C can be attributed to both $Fe_2O_3 \rightarrow Fe_3O_4$ and $MnO_2 \rightarrow Mn_2O_3$. Meanwhile, the third peak for the MnO_x/VMT sample located at 608 °C can be attributed to $Fe_3O_4 \rightarrow FeO$, and the forth peak located at 742 °C can be attributed to $FeO \rightarrow Fe$ [54]. The H_2-TPR curve for the MnO_x-Fe_2O_3/VMT catalyst exhibited similar reduction peaks above 260 °C, but which were shifted to lower temperatures relative to those for the MnO_x/VMT catalyst, suggesting that the Fe and Mn species in the MnO_x-Fe_2O_3/VMT catalyst were more easily reduced. This can be ascribed to the previously discussed synergetic effect between Mn and Fe, which could effectively promote the redox properties of the MnO_x-Fe_2O_3/VMT catalyst and improve its catalytic activity.

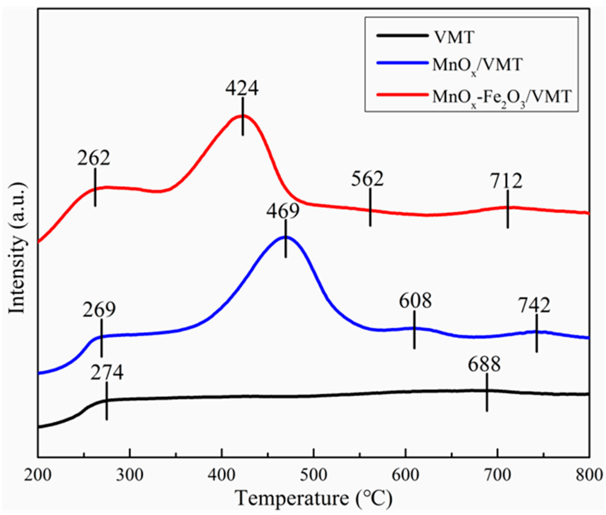

Figure 4. H_2-TPR curves of the VMT support and MnO_x/VMT and MnO_x-Fe_2O_3/VMT catalyst samples.

A photograph of the as-prepared MnO_x-Fe_2O_3/VMT MHCs is shown in Figure 5a. The macrostructure of the MnO_x-Fe_2O_3/VMT MHCs is important for promoting catalytic activity in industrial applications, and their primary physical properties have significant effects on their mechanical and catalytic performances. The SEM micrograph of an as-prepared MnO_x-Fe_2O_3/VMT MHCs in Figure 5b shows that the glass fibers were uniformly distributed throughout the MnO_x-Fe_2O_3/VMT MHCs, which can be expected to provide enhanced mechanical strength. The XRD pattern of a representative MnO_x-Fe_2O_3/VMT MHCs is shown in Figure 5c. In contrast with the XRD results for the MnO_x-Fe_2O_3/VMT powdered catalyst (Figure 2a), the bentonite content in the MHCs, which has a large proportion of SiO_2, yields a sharp peak attributable to SiO_2 (PDF#27-0605) at 21.6°. In addition, two sharp peaks attributable to carbon (PDF#41-1487) are observed at 26.4° and 54.5° owing to the decomposition of the organic additives. Figure 5d presents the N_2 isotherms and corresponding pore size distribution curve (inset) of a MnO_x-Fe_2O_3/VMT MHCs, and the corresponding textural data are listed Table 1. Here, we note that, while the BET surface area and poor volume of the MnO_x-Fe_2O_3/VMT MHCs were less than those of its powdered counterpart, the average pore diameter was increased by around 10%. The porous texture of the MnO_x-Fe_2O_3/VMT MHCs can be expected to play a significant role in the SCR of NO_x owing to an enhanced transportation and adsorption of reactant gases.

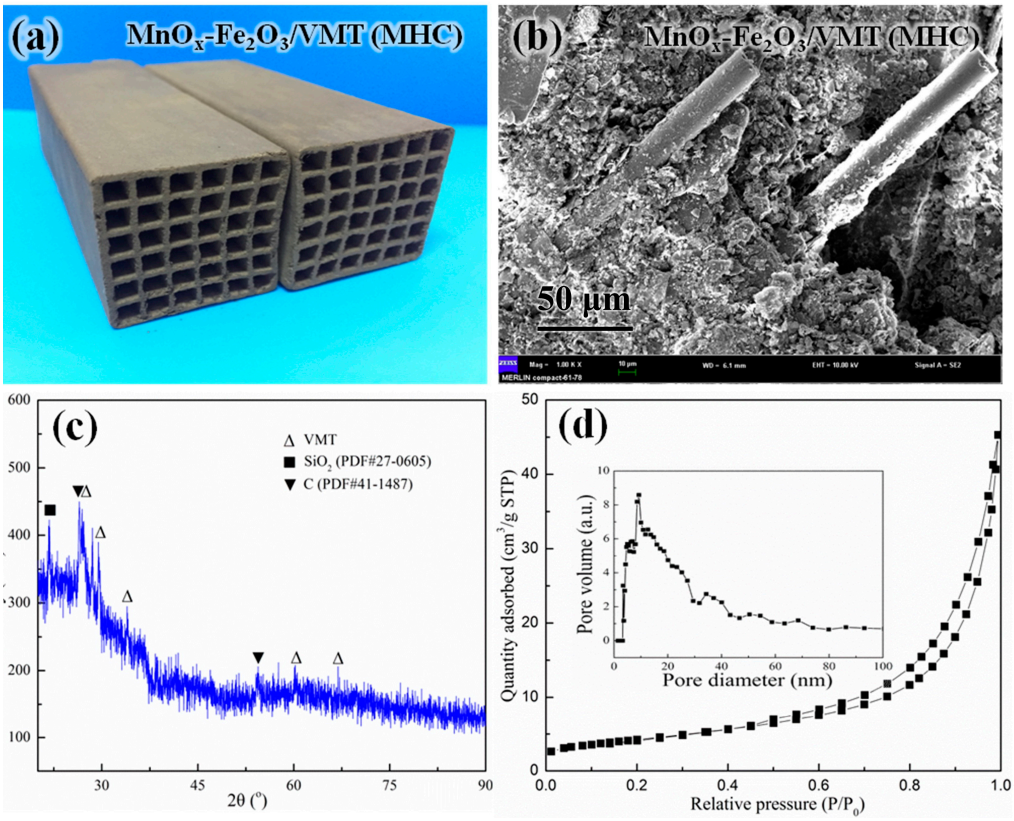

Figure 5. MnO_x-Fe_2O_3/VMT MHCs: (**a**) photograph of as-prepared MHCs; (**b**) SEM image; (**c**) XRD pattern; (**d**) N_2 isotherms and corresponding pore size distribution curve (inset).

The NO conversion of MnO_x-Fe_2O_3/VMT MHCs at different GHSV values is shown as a function of reaction temperature in Figure 6a. We note that the NO conversion decreased with an increasing GHSV from 4000 h^{-1} to 8000 h^{-1}. The temperature region of highest activity was between 150 °C and 200 °C, and the NO conversion attained a maximum value greater than 98% with GHSV = 4000 h^{-1}. Meanwhile, the MnO_x-Fe_2O_3/VMT MHCs exhibited an excellent NO conversion of 39.2% and 53.4% at 20 °C and 50 °C, respectively, with GHSV = 4000 h^{-1}. The cycling stabilities of MnO_x-Fe_2O_3/VMT

MHCs are presented in Figure 6b at various temperatures with different GHSV values. We note that the NO conversion was stable, with no significant changes over a full 10 h of testing. We also find that the MnO_x-Fe_2O_3/VMT MHCs provided excellent NO conversion values of 98.6% and 85.8% at 150 °C and 100 °C, respectively, with GHSV = 4000 h^{-1}. The results obtained are comparable to those reported in the literature (Figure 6c). Thus, a NO conversion of 92% at 500 °C has been reported for WO_3-TiO_2 (GHSV of 11,000 h^{-1}) [55], a conversion of 98% at 400 °C was reached by V_2O_5-MoO_3/TiO_2 (GHSV of 6000 h^{-1}) [56]. A TiO_2 catalyst showed a conversion of 80% at 300 °C (GHSV of 25,000 h^{-1}) [57], 75% at 250 °C for a V_2O_5-WO_3/TiO_2 catalyst (GHSV of 27,000 h^{-1}) [58], and 90% at 160 °C for a Cr-V/TiO_2 catalyst (GHSV of 4000 h^{-1}) [59]. Even at GHSV = 2000 h^{-1}, the MnO_x-Fe_2O_3/VMT MHCs provided an NO conversion of 79.1% at 50 °C. Surprisingly, the MHCs exhibited excellent NO conversion values of 62.2% and 50.2% with GHSV = 1000 h^{-1} and 2000 h^{-1}, respectively, at 20 °C. The excellent SCR performance obtained for the proposed MnO_x-Fe_2O_3/VMT MHCs will strongly contribute to low-temperature De-NO_x processes, and suggests that even room temperature processes are feasible.

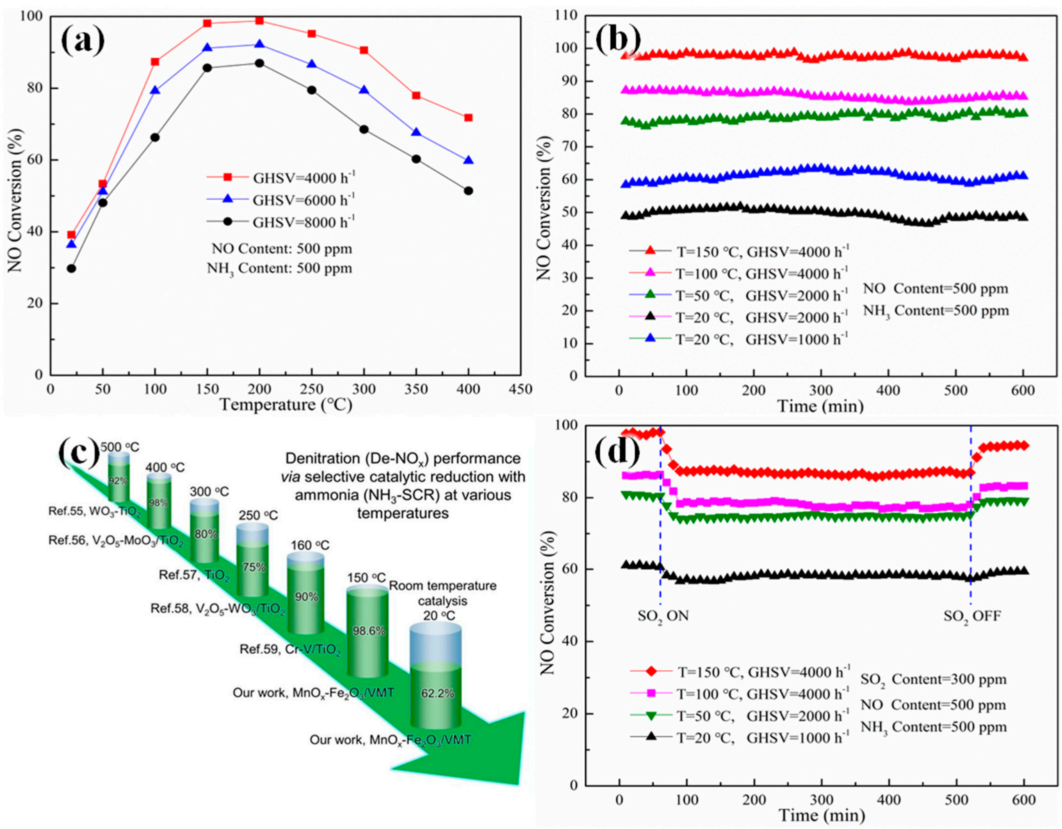

Figure 6. Catalytic activity of MnO_x-Fe_2O_3/VMT MHCs: (**a**) NO conversion; (**b**) cycling stabilities; (**c**) Comparison of pervious reported activity of various MHCs for NH_3-SCR; (**d**) SO_2 resistance at various temperatures with different GHSV.

The impact of SO_2 on the cycling performance of MnO_x-Fe_2O_3/VMT MHCs at different temperatures and GHSV values is shown in Figure 6d. After the first 1 h of testing when 300 ppm SO_2 was introduced into the reaction gas, we note that the extent to which the NO conversion decreased was only slight at 20 °C (GHSV = 1000 h^{-1}), but increased with increasing temperature from 50 °C (GHSV = 2000 h^{-1}) to 150 °C (GHSV = 4000 h^{-1}). This is because the crystallization temperature of sulfate is greater than 40 °C. We also note that the NO conversion of the MnO_x-Fe_2O_3/VMT MHCs was stable over the entire period of SO_2 addition, which indicates good SO_2 resistance. However, the NO conversion values obtained under all conditions did not recover to their original values when the addition of SO_2 was discontinued. These results suggest that the decreased activity of the MHCs was not due to the competitive adsorption of SO_2, but because of the formation of sulfates covering the active sites of the catalysts [60].

3. Materials and Methods

3.1. Catalysts Preparation

3.1.1. Preparation of MnO_x/VMT and MnO_x-Fe_2O_3/VMT Catalysts

Vermiculite supports were prepared by a microwave method as follows. The raw VMT (Xinjiang Yuli Xinlong Vermiculite Co., Ltd., Korla, China) was washed with water until no trace of foreign material was observable under visual inspection, and then dried in an oven at 100 °C. Finally, the washed VMT was placed in a 500 mL beaker and expanded in a microwave. The VMT was collected and placed in a sealed container, and then crushed prior to use. All the catalysts were prepared by the impregnation method. We completely dissolved $Mn(CH_3COO)_2 \cdot 4H_2O$ in water under stirring in an appropriate ratio to the VMT content (i.e., 20 wt% Mn). We added the VMT powder, and continued stirring for 10 h. The sample was dried in air at 100 °C for 12 h, and then crushed and sieved in an 80–100 mesh sieve. Finally, the sample was calcined in air at 500 °C for 5 h. We prepared MnO_x-Fe_2O_3/VMT catalysts by an equivalent method using $Mn(CH_3COO)_2 \cdot 4H_2O$ and $Fe(NO_3)_3 \cdot 9H_2O$ (20 wt% Mn-5 wt% Fe relative to VMT).

3.1.2. Preparation of MnO_x-Fe_2O_3/VMT Monolithic Honeycomb Catalysts

We synthesized MnO_x-Fe_2O_3/VMT MHCs by an extrusion molding method. The powdered MnO_x-Fe_2O_3/VMT catalyst was dry mixed with 10 wt% bentonite and 3 wt% carboxy methyl cellulose (CMC) in a blender mixer. The materials in the blender mixer were then wet mixed with 10 wt% glycerin, followed by a sufficient amount of water to ensure an appropriate viscosity for extrusion. The resulting mixture was kneaded by hand for 30 min until achieving a uniform consistency. The sample was subjected to vacuum de-airing and aged for 24 h to increase the plasticity. The aged sample was molded by an extruding machine to obtain a monolithic honeycomb structure. The honeycomb sample was dried at 70 °C in air for 12 h in a muffle furnace, further dried at 100 °C for 12 h, and then calcined at 500 °C for 5 h. The rate of temperature increase was 1 °C/min for all the above steps. The mold size was 3.3 cm × 3.3 cm with 36 channels (i.e., 6 × 6 cells).

3.2. Catalyst Characterization

The morphologies of the powder catalysts and MHCs were characterized by scanning electron microscopy (SEM; Hitachi S-4300, Hitachi Limited, Tokyo, Japan). A BET apparatus (Micromeritics ASAP 2020, Micromeritics Instrument Ltd., Norcross, GA, USA) was employed to measure the Brunauer-Emmett-Teller (BET) specific surface area and Barrett-Joyner-Halenda (BJH) pore structure of the powder catalysts and MHCs. The samples were degassed in vacuum at 200 °C for 4 h prior to measurement. The total pore volume was calculated from the volume of nitrogen adsorbed at $P/P_0 = 0.99$. Powder X-ray diffraction (XRD) patterns were recorded on a Bruker D8 Advance X-ray diffractometer (Bruker Biosciences Corporation, Billerica, MA, USA) with Cu Kα radiation (λ = 1.5406 Å) operated at 40 kV and 40 mA. X-ray photoelectron spectroscopy (XPS) data were obtained with an AMICUS/ESCA 3400 electron spectrometer from Kratos Analytical (Manchester, UK) using Mg Kα radiation (20 mA, 12 kV). Binding energies were referenced to the C 1s line at 284.8 eV for adventitious carbon. We conducted H_2 temperature programmed reduction (H_2-TPR) testing to analyze the redox properties of the catalysts using a Micromeritics ChemiSorb 2720TPx system (Micromeritics Instrument Ltd., Norcross, GA, USA) in a temperature range of 20 °C to 800 °C at a rate of 10 °C/min with a gas (10 vol% H_2 relative to Ar) flow rate of 40 mL/min, and then retained for 20 min at 800 °C.

3.3. Activity Measurement

We prepared MnO_x/VMT and MnO_x-Fe_2O_3/VMT catalytic activity studies using a fixed bed microreactor. The reactor was composed of a stainless steel tube with a 10.0 mm inner diameter. Prior to conducting the experiments, quartz sand and quartz wool were placed inside the reaction tube to ensure contact between the powdered catalysts and the thermocouple. The typical composition of the simulated flue gas was 500 ppm NO (denoted as $[NO]_{in}$), 500 ppm NH_3 (denoted as $[NH_3]_{in}$), and 5 vol% O_2 with N_2 as the balance gas. The total volume flow was 100 mL/min, representing a GHSV of 30,000 h^{-1}. The catalytic activity of the powdered catalysts was evaluated in the temperature range of 20 °C to 400 °C during testing according to the exiting concentrations of NO (denoted as $[NO]_{out}$) and NH_3 (denoted as $[NH_3]_{out}$) determined by Fourier transform infrared (FTIR) spectroscopy (Nicolet IS10, Thermo Fisher Scientific, Waltham, MA, USA). The NO conversion ($[NO]_{conversion}$) and N_2 selectivity ($[N_2]_{selectivity}$) were calculated using the following equations:

$$[NO]_{conversion} = \frac{[NO]_{in} - [NO]_{out}}{[NO]_{in}} \times 100\% \quad (1)$$

$$[N_2]_{selectivity} = \left[1 - \frac{[NO_2]_{out} + 2[N_2O]_{out}}{[NO]_{in} - [NO]_{out} + [NH_3]_{in} - [NH_3]_{out}}\right] \times 100\% \quad (2)$$

The catalytic performance of MnO_x-Fe_2O_3/VMT MHCs was evaluated using a similar fixed bed microreactor composed of a quartz tube with a 5.0 cm inner diameter. The simulated flue gas was composed of 500 ppm NO and 500 ppm NH_3 with air as the balance gas. Prior to testing, each MHCs sample was placed in the reaction tube, and then exposed to the simulated flue gas for 1 h to eliminate the influence of adsorption on the catalysts. Then, $[NO]_{out}$ was measured online using a flue gas analyzer (QUINTOX-KM9106, Kane International, New York, NY, USA), and $[NO]_{conversion}$ was calculated using Equation (1). Unless otherwise stated here, all other conditions were equivalent to the conditions employed for powdered catalysts.

4. Conclusions

This paper presented the successful preparation of MnO_x-Fe_2O_3/VMT catalysts with a layered structure by an impregnation method for the first time. The as-prepared MnO_x-Fe_2O_3/VMT catalysts exhibited high NO conversion and N_2 selectivity for the NH_3-SCR of NO in the temperature range of 20–200 °C. The catalysts provided an excellent NO conversion of 96.5% at 200 °C with GHSV = 30,000 h^{-1} and an NO concentration of 500 ppm. Compared with VMT and MnO_x/VMT catalysts, the results of extensive characterization indicated that the high catalytic activity of the MnO_x-Fe_2O_3/VMT catalysts can be attributed to a number of advantageous properties, such as a large specific surface area, high ratios of Mn^{4+}/Mn_{total} and Fe^{3+}/Fe_{total}, and easily reduced Mn species. In addition, the MnO_x-Fe_2O_3/VMT powdered catalyst was successfully employed to form MHCs by an extrusion method. The as-prepared MnO_x-Fe_2O_3/VMT MHCs provided an NO conversion of 98.6% at 150 °C with GHSV = 4000 h^{-1}. Moreover, the MHCs presented excellent De-NO_x performance at low temperature, obtaining an NO conversion of 62.2% at 20 °C with GHSV = 1000 h^{-1}. Furthermore, the MnO_x-Fe_2O_3/VMT MHCs also provided excellent cycling stability, and maintained comparable NO conversion values even after 10 h. Finally, the MnO_x-Fe_2O_3/VMT MHCs demonstrated excellent SO_2 resistance at low temperature (particularly at room temperature). Therefore, the prepared MnO_x-Fe_2O_3/VMT MHCs offer considerable potential for low or even room temperature De-NO_x applications in stationary stack source emissions.

Acknowledgments: The work was supported by National High Technology Research and Development Program of China (863 program) (no. 2015AA03A401), Program for Changjiang Scholars and Innovative Research Team in University (no. IRT_15R46) and the Program of Science and Technology Innovation Team in Bingtuan (no. 2015BD003).

Author Contributions: F.Y. and B.D. designed and administered the experiments. K.Z. performed experiments. M.Z., J.D., X.W., and J.Z. collected and analyzed data. All authors discussed the data and wrote the manuscript.

Conflicts of Interest: The authors declare no conflicts of interests.

References

1. Cai, S.; Liu, J.; Zha, K.; Li, H.; Shi, L.; Zhang, D. A general strategy for the in situ decoration of porous Mn-Co bi-metal oxides on metal mesh/foam for high performance de-NO_x monolith catalysts. *Nanoscale* **2017**, *9*, 5648–5657. [CrossRef] [PubMed]
2. Boningari, T.; Smirniotis, P.G. Impact of nitrogen oxides on the environment and human health: Mn-based materials for the NO_x abatement. *Curr. Opin. Chem. Eng.* **2016**, *13*, 133–141. [CrossRef]
3. Li, J.H.; Chang, H.Z.; Ma, L.; Hao, J.M.; Yang, R.T. Low-temperature selective catalytic reduction of NO_x with NH_3 over metal oxide and zeolite catalysts—A review. *Catal. Today* **2011**, *175*, 147–156. [CrossRef]
4. Zhu, Y.; Chen, B.; Zhao, R.; Zhao, Q.; Gies, H.; Xiao, F.; Vos, D.E.D.; Yokoi, T.; Bao, X.; Kolb, U.; et al. Fe-doped Beta Zeolite from Organotemplate-free Synthesis for NH_3-SCR of NO_x. *Catal. Sci. Technol.* **2016**, *6*, 6581–6592. [CrossRef]
5. Liu, C.; Shi, J.W.; Niu, C. Manganese oxide-based catalysts for low-temperature selective catalytic reduction of NO_x with NH_3: A review. *Appl. Catal. A Gen.* **2016**, *522*, 54–69. [CrossRef]
6. Long, R.Q.; Yang, R.T.; Chang, R. Low temperature selective catalytic reduction (SCR) of NO with NH_3 over Fe-Mn based catalysts. *Chem. Commun.* **2012**, *5*, 452–453.
7. Boningari, T.; Pappas, D.K.; Ettireddy, P.R.; Kotrba, A.; Smirniotis, P.G. Influence of SiO_2 on M/TiO_2 M = Cu, Mn, and Ce) formulations for low-temperature selective catalytic reduction of NO_x with NH_3: Surface properties and key components in relation to the activity of NO_x reduction. *Ind. Eng. Chem. Res.* **2015**, *54*, 2261–2273. [CrossRef]
8. Chen, Z.; Wang, F.; Li, H.; Yang, Q.; Wang, L.F.; Li, X.H. Low-Temperature Selective Catalytic Reduction of NO_x with NH_3 over Fe–Mn Mixed-Oxide Catalysts Containing $Fe_3Mn_3O_8$ Phase. *Ind. Eng. Chem. Res.* **2012**, *51*, 202–212. [CrossRef]
9. Li, R.; Li, Z.B.; Chen, L.Q.; Dong, Y.L.; Ma, S.B.; Yuan, F.L.; Zhu, Y.J. Synthesis of MnNi–SAPO-34 by a one-pot hydrothermal method and its excellent performance for the selective catalytic reduction of NO by NH_3. *Catal. Sci. Technol.* **2017**, *7*, 4989–4995. [CrossRef]
10. Lou, X.; Liu, P.; Li, J.; Li, Z.; He, K. Effects of calcination temperature on Mn species and catalytic activities of Mn/ZSM-5 catalyst for selective catalytic reduction of NO with ammonia. *Appl. Sur. Sci.* **2014**, *307*, 382–387. [CrossRef]
11. Yu, C.; Dong, L.; Feng, C.; Liu, X.; Huang, B. Low-temperature SCR of NO_x by NH_3 over MnO_x/SAPO-34 prepared by two different methods: A comparative study. *Environ. Technol.* **2017**, *38*, 1030–1042. [CrossRef] [PubMed]
12. Liu, J.; Zhang, K.; Si, M.; Lian, J.H.; Liu, L.S.; Gou, X. Experimental Research on Catalysts of V_2O_5/AC and V_2O_5/CNTs for Low Temperature SCR Denitrification. *Appl. Mech. Mater.* **2014**, *694*, 478–483. [CrossRef]
13. Lu, X.; Zheng, Y.; Zhang, Y.; Qiu, H. Low-temperature selective catalytic reduction of NO over carbon nanotubes supported MnO_2 fabricated by co-precipitation method. *Micro Nano Lett.* **2015**, *10*, 666–669. [CrossRef]
14. Lin, F.; Wu, X.; Liu, S.; Weng, D.; Huang, Y. Preparation of MnO_x–CeO_2–Al_2O_3 mixed oxides for NO_x-assisted soot oxidation: Activity, structure and thermal stability. *Chem. Eng. J.* **2013**, *226*, 105–112. [CrossRef]
15. Jin, R.; Liu, Y.; Wu, Z.; Wang, H.; Gu, T. Low-temperature selective catalytic reduction of NO with NH_3 over MnCe oxides supported on TiO_2 and Al_2O_3: A comparative study. *Chemosphere* **2010**, *78*, 1160–1166. [CrossRef] [PubMed]
16. Pappas, D.K.; Boningari, T.; Boolchand, P.; Smirniotis, P.G. Novel manganese oxide confined interweaved titania nanotubes for the low-temperature selective catalytic reduction (SCR) of NO_x by NH_3. *J. Catal.* **2016**, *334*, 1–13. [CrossRef]
17. Ettireddy, P.R.; Ettireddy, N.; Boningari, T.; Pardemann, R.; Smirniotis, P.G. Investigation of the selective catalytic reduction of nitric oxide with ammonia over Mn/TiO_2 catalysts through transient isotopic labeling and in situ FT-IR studies. *J. Catal.* **2012**, *292*, 53–63. [CrossRef]

18. Smirniotis, P.G.; Peña, D.A.; Uphade, B.S. Low-Temperature Selective Catalytic Reduction (SCR) of NO with NH_3 by Using Mn, Cr, and Cu Oxides Supported on Hombikat TiO_2. *Angew. Chem. Int. Ed. Eng.* **2001**, *40*, 2479–2482. [CrossRef]
19. Singoredjo, L.; Korver, R.; Kapteijn, F.; Moulijn, J. Alumina supported manganese oxides for the low-temperature selective catalytic reduction of nitric oxide with ammonia. *Appl. Catal. B* **1992**, *1*, 297–316. [CrossRef]
20. Ma, K.; Zou, W.X.; Zhang, L.; Li, L.L.; Yu, S.H.; Tang, C.J.; Gao, F.; Dong, L. Construction of hybrid multi-shell hollow structured CeO_2-MnO_x materials for selective catalytic reduction of NO with NH_3. *RSC Adv.* **2017**, *7*, 5989–5999. [CrossRef]
21. Liu, C.; Gao, G.; Shi, J.W.; He, C.; Li, G.D.; Bai, N.; Niu, C. MnO_x-CeO_2 shell-in-shell microspheres for NH_3-SCR de-NO_x at low temperature. *Catal. Commun.* **2016**, *86*, 36–40. [CrossRef]
22. Qi, G.; Yang, R.T.; Chang, R. MnO_x-CeO_2 mixed oxides prepared by co-precipitation for selective catalytic reduction of NO with NH_3 at low temperatures. *Appl. Catal. B Environ.* **2004**, *51*, 93–106. [CrossRef]
23. Hu, H.; Zha, K.; Li, H.; Shi, L.; Zhang, D. In situ DRIFTs investigation of the reaction mechanism over MnO_x-$MO_y/Ce_{0.75}Zr_{0.25}O_2$ (M = Fe, Co, Ni, Cu) for the selective catalytic reduction of NO_x with NH_3. *Appl. Sur. Sci.* **2016**, *387*, 921–928. [CrossRef]
24. Xiao, F.; Gu, Y.; Tang, Z.; Han, F.; Shao, J.; Xu, Q.; Zhu, H. ZrO_2 Modified MnO_x/Attapulgite Catalysts for NH_3-SCR of NO at Low Temperature. *J. Chem. Eng. Jpn.* **2015**, *48*, 481–487. [CrossRef]
25. Xie, A.; Zhou, X.; Huang, X.; Ji, L.; Zhou, W.; Luo, S.; Yao, C. Cerium-loaded MnO_x/attapulgite catalyst for the low-temperature NH_3-selective catalytic reduction. *J. Ind. Eng. Chem.* **2017**, *49*, 230–241. [CrossRef]
26. Chmielarz, L.; Kuśtrowski, P.; Dziembaj, R.; Cool, P.; Vansant, E.F. Selective catalytic reduction of NO with ammonia over porous clay heterostructures modified with copper and iron species. *Catal. Today* **2007**, *119*, 181–186. [CrossRef]
27. Hou, X.X.; Schmieg, S.J.; Wei, L.; Epling, W.S. NH_3 pulsing adsorption and SCR reactions over a Cu-CHA SCR catalyst. *Catal. Today* **2012**, *197*, 9–17. [CrossRef]
28. Schmieg, S.J.; Oh, S.H.; Kim, C.H.; Brown, D.B.; Lee, J.H.; Pedenc, C.H.F.; Kim, D.H. Thermal durability of Cu-CHA NH_3-SCR catalysts for diesel NO_x reduction. *Catal. Today* **2012**, *184*, 252–261. [CrossRef]
29. Brookshear, D.W.; Nam, J.G.; Ke, N.; Toops, T.J.; Binder, A. Impact of sulfation and desulfation on NO_x reduction using Cu-chabazite SCR catalysts. *Catal. Today* **2015**, *258*, 359–366. [CrossRef]
30. Luo, S.; Zhou, W.; Xie, A.; Wu, F.; Yao, C.; Li, X.; Zuo, S.; Liu, T. Effect of MnO_2 polymorphs structure on the selective catalytic reduction of NO_x with NH_3 over TiO_2–Palygorskite. *Chem. Eng. J.* **2016**, *286*, 291–299. [CrossRef]
31. Chmielarz, L.; Kuśtrowski, P.; Piwowarska, Z.; Dudek, B.; Gil, B.; Michalik, M. Montmorillonite, vermiculite and saponite based porous clay heterostructures modified with transition metals as catalysts for the $DeNO_x$ process. *Appl. Catal. B Environ.* **2009**, *88*, 331–340. [CrossRef]
32. Samojeden, B.; Możdżeń, M. The influence of amount of copper of modified vermiculites on catalytic properties in SCR-NH_3. *Energy Fuels* **2017**, *14*, 02020. [CrossRef]
33. Ying, S. Preparation and Properties of Vermiculite Supported TiO_2 Photocatalyst. *Chin. J. Inorg. Chem.* **2011**, *27*, 40–46.
34. Li, P.; Zhu, M.; Dan, J.; Kang, L.; Lai, L.; Cai, X.; Zhang, J.; Yu, F.; Tian, Z.; Dai, B. Two-dimensional porous SiO_2 nanomesh supported high dispersed Ni nanoparticles for CO methanation. *Chem. Eng. J.* **2017**, *326*, 774–780. [CrossRef]
35. Li, P.; Wen, B.; Yu, F.; Zhu, M.; Guo, X.; Han, Y.; Kang, L.; Huang, X.; Dan, J.; Ouyang, F.; et al. High efficient nickel/vermiculite catalyst prepared via microwave irradiation-assisted synthesis for carbon monoxide methanation. *Fuel* **2016**, *171*, 263–269. [CrossRef]
36. Huang, X.; Yu, F.; Zhu, M.; Ouyang, F.; Dan, J. Hydrochlorination of acetylene using expanded multilayered vermiculite (EML-VMT)-supported catalysts. *Chin. Chem. Lett.* **2015**, *26*, 1101–1104. [CrossRef]
37. Shen, B.; Liu, T.; Zhao, N.; Yang, X.; Deng, L. Iron-doped Mn-Ce/TiO_2 catalyst for low temperature selective catalytic reduction of NO with NH_3. *J. Environ. Sci. Chin.* **2010**, *22*, 1447–1454. [CrossRef]
38. Lin, Q.; Li, J.; Ma, L.; Hao, J. Selective catalytic reduction of NO with NH_3 over Mn–Fe/USY under lean burn conditions. *Catal. Today* **2010**, *151*, 251–256. [CrossRef]

39. Thirupathi, B.; Smirniotis, P.G. Co-doping a metal (Cr, Fe, Co, Ni, Cu, Zn, Ce, and Zr) on Mn/TiO_2 catalyst and its effect on the selective reduction of NO with NH_3 at low-temperatures. *Appl. Catal. B Environ.* **2011**, *110*, 195–206. [CrossRef]
40. Fan, Z.; Shi, J.W.; Gao, C.; Gao, G.; Wang, B.; Niu, C. Rationally Designed Porous MnO_x-FeO_x Nanoneedles for Low-Temperature Selective Catalytic Reduction of NO_x by NH_3. *ACS Appl. Mater. Interfaces* **2017**, *9*, 16117. [CrossRef] [PubMed]
41. Thirupathi, B.; Smirniotis, P.G. Nickel-doped Mn/TiO_2 as an efficient catalyst for the low-temperature SCR of NO with NH_3: Catalytic evaluation and characterizations. *J. Catal.* **2012**, *288*, 74–83. [CrossRef]
42. Kapteijn, F.; Singoredjo, L.; Andreini, A.; Moulijn, J.A. Activity and selectivity of pure manganese oxides in the selective catalytic reduction of nitric oxides with ammonia. *Appl. Catal. B Environ.* **1994**, *3*, 173–189. [CrossRef]
43. Reddy, G.K.; He, J.; Thiel, S.W.; Pinto, N.G.; Smirniotis, P.G. Sulfur-tolerant Mn-Ce-Ti sorbents for elemental mercury removal from flue gas: Mechanistic investigation by XPS. *J. Phys. Chem. C* **2015**, *119*, 8634–8644. [CrossRef]
44. Gao, G.; Shi, J.W.; Liu, C.; Gao, C.; Fan, Z.; Niu, C. Mn/CeO_2 catalysts for SCR of NO_x with NH_3: Comparative study on the effect of supports on low-temperature catalytic activity. *Appl. Sur. Sci.* **2017**, *411*, 338–346. [CrossRef]
45. Li, Y.; Wan, Y.; Li, Y.; Zhan, S.; Guan, Q.; Tian, Y. Low-Temperature Selective Catalytic Reduction of NO with NH_3 over Mn_2O_3-doped Fe_2O_3 Hexagonal Microsheets. *ACS Appl. Mater. Interfaces* **2016**, *8*, 5224–5233. [CrossRef] [PubMed]
46. Zhang, J.; Qu, H. Low-temperature selective catalytic reduction of NO_x with NH_3 over Fe–Cu mixed oxide/ZSM-5 catalysts containing Fe_2CuO_4 phase. *Res. Chem. Interfaces* **2015**, *41*, 4961–4975. [CrossRef]
47. Lin, Z.; Lei, Z.; Qu, H.; Qin, Z. A study on chemisorbed oxygen and reaction process of Fe-CuO_x/ZSM-5 via ultrasonic impregnation method for low-temperature NH_3-SCR. *J. Mol. Catal. A Chem.* **2015**, *409*, 207–215.
48. Haidi, X.U.; Fang, Z.; Cao, Y.; Kong, S.; Lin, T.; Gong, M.; Chen, Y. Influence of Mn/(Mn + Ce) Ratio of MnO_x-CeO_2/WO_3-ZrO_2 Monolith Catalyst on Selective Catalytic Reduction of NO_x with Ammonia. *Chin. J. Catal.* **2012**, *33*, 1927–1937.
49. Fang, C.; Zhang, D.; Cai, S.; Zhang, L.; Huang, L.; Li, H.; Maitarad, P.; Shi, L.; Gao, R.; Zhang, J. Low-temperature selective catalytic reduction of NO with NH_3 over nanoflaky MnO_x on carbon nanotubes in situ prepared via a chemical bath deposition route. *Nanoscale* **2013**, *5*, 9199–9207. [CrossRef] [PubMed]
50. Boningari, T.; Ettireddy, P.R.; Somogyvari, A.; Liu, Y.; Vorontsov, A.; Mcdonald, C.A.; Smirniotis, P.G. Influence of elevated surface texture hydrated titania on Ce-doped Mn/TiO_2 catalysts for the low-temperature SCR of NO_x under oxygen-rich conditions. *J. Catal.* **2015**, *325*, 145–155. [CrossRef]
51. Khan, A.; Smirniotis, P.G. Relationship between temperature-programmed reduction profile and activity of modified ferrite-based catalysts for WGS reaction. *J. Mol. Catal. A Chem.* **2008**, *280*, 43–51. [CrossRef]
52. Cai, S.; Hu, H.; Li, H.; Shi, L.; Zhang, D. Design of multi-shell Fe_2O_3@MnO_x@CNTs for the selective catalytic reduction of NO with NH_3: Improvement of catalytic activity and SO_2 tolerance. *Nanoscale* **2016**, *8*, 3588–3598. [CrossRef] [PubMed]
53. Liu, Z.; Zhu, J.; Li, J.; Ma, L.; Woo, S.I. Novel Mn-Ce-Ti mixed-oxide catalyst for the selective catalytic reduction of NO_x with NH_3. *ACS Appl. Mater. Interfaces* **2014**, *6*, 14500–14508. [CrossRef] [PubMed]
54. France, L.J.; Yang, Q.; Li, W.; Chen, Z.; Guang, J.; Guo, D.; Wang, L.F.; Li, X.H. Ceria modified $FeMnO_x$-Enhanced performance and sulphur resistance for low-temperature SCR of NO_x. *Appl. Catal. B Environ.* **2017**, *206*, 203–215. [CrossRef]
55. Kobayashi, M.; Miyoshi, K. WO_3–TiO_2 monolithic catalysts for high temperature SCR of NO by NH_3: Influence of preparation method on structural and physico-chemical properties, activity and durability. *Appl. Catal. B Environ.* **2007**, *72*, 253–261. [CrossRef]
56. Qiu, Y.; Liu, B.; Du, J.; Tang, Q.; Liu, Z.; Liu, R.; Tao, C. The monolithic cordierite supported V_2O_5–MoO_3/TiO_2 catalyst for NH_3-SCR. *Chem. Eng. J.* **2016**, *294*, 264–272. [CrossRef]
57. Hwang, J.; Ha, H.J.; Ryu, J.; Choi, J.J.; Ahn, C.W.; Kim, J.W.; Hahn, B.D.; Yoon, W.H.; Lee, H.; Choi, J.H. Enhancement of washcoat adhesion for SCR catalysts to convert nitrogen oxide using powder spray coating of TiO_2 on metallic honeycomb substrate. *Catal. Commun.* **2017**, *94*, 1–4. [CrossRef]

58. Gan, L.; Lei, S.; Yu, J.; Ma, H.; Yamamoto, Y.; Suzuki, Y.; Xu, G.; Zhang, Z. Development of highly active coated monolith SCR catalyst with strong abrasion resistance for low-temperature application. *Front. Environ. Sci. Eng.* **2015**, *9*, 979–987. [CrossRef]
59. Huang, H.F.; Jin, L.L.; Lu, H.F.; Yu, H.; Chen, Y.J. Monolithic Cr–V/TiO_2/cordierite catalysts prepared by in-situ precipitation and impregnation for low-temperature NH_3-SCR reactions. *Catal. Commun.* **2013**, *34*, 1–4. [CrossRef]
60. Gao, C.; Shi, J.W.; Fan, Z.; Niu, C. Sulfur and Water Resistance of Mn-Based Catalysts for Low-Temperature Selective Catalytic Reduction of NO_x: A Review. *Catalysts* **2018**, *8*, 11. [CrossRef]